ELSEVIER

Surface Science 486 (2001) 167–184

SURFACE SCIENCE

www.elsevier.nl/locate/susc

The evolution of Ni nanoislands on the rutile $TiO_2(110)$ surface with coverage, heating and oxygen treatment

R.E. Tanner [a,*], I. Goldfarb [b], M.R. Castell [a], G.A.D. Briggs [a]

[a] *Department of Materials, University of Oxford, Parks Road, Oxford OX1 3PH, UK*

[b] *Department of Solid Mechanics, Materials and Structures, The Iby and Aladar Fleischman, Faculty of Engineering, Tel Aviv University, 69978 Ramat Aviv, Israel*

Received 8 September 2000; accepted for publication 16 March 2001

Abstract

Scanning tunnelling microscopy (STM) and reflection high-energy electron diffraction (RHEED) have been used to examine in situ the morphology and growth of nickel nanoislands on the rutile $TiO_2(110)$-p(1 × 1) surface. Such analysis revealed growth at temperatures between 295 and 495 K via the Volmer–Weber (V–W) mode of three-dimensional islands, in agreement with thermodynamic expectations. The Ni islands grew first as small crystalline domes with no preferential alignment with the $TiO_2(110)$ surface, but with increasing Ni dose their orientation evolved, until almost perfect monocrystalline $(110)_{Ni}\|(110)_{TiO_2}$, $[\bar{1}10]_{Ni}\|[001]_{TiO_2}$ orientation-relations were established. This arrangement has one of the lowest lattice mismatches if an average of the two orthogonal surface directions $[001]_{TiO_2}$ and $[110]_{TiO_2}$ is considered. The epitaxial relation persists upon annealing in ultra-high vacuum (UHV) to 1065 K and the heat treatment causes the particles to coarsen and grow in size. When the crystalline islands of nickel are oxidised, the lattice parameters are modified, consistent with the formation of NiO. A new epitaxial relation is established between the overlayer and the substrate: $(001)_{layer}\|(110)_{TiO_2}$, $[1\bar{1}0]_{layer}\|[001]_{TiO_2}$. This produces a large strain parallel to the $[1\bar{1}0]_{TiO_2}$ direction and a very small strain along $[001]_{TiO_2}$ (+0.13% mismatch). UHV annealing of the oxidised overlayer reduces the crystallites to islands with lattice parameters corresponding to nickel metal, but the original crystallography is not recovered. Instead, the nanoislands of reduced nickel maintain the same overlayer orientation as for the oxide. A model is presented in which the change in epitaxial relation is attributed to the formation of an interfacial NiO layer between the reduced Ni islands and TiO_2 substrate. The results demonstrate that the oxidation/reduction treatment of the substrate and overlayer can be used to modify the microstructure of the metal/oxide system, and have implications for the use of nickel as a supported metal catalyst.

Keywords: Nickel; Titanium oxide; Scanning tunneling microscopy; Reflection high-energy electron diffraction (RHEED); Epitaxy; Growth; Surface structure, morphology, roughness, and topography; Oxidation

1. Introduction

Despite the advances in catalyst technology since the discovery of nickels catalytic activity (as early as 1869), nickel has not been superseded as the material of choice for the hydrogenation of oils

* Corresponding author. Present address: Department of Chemical Engineering, Yale University, P.O. Box 208286, New Haven, CT 06520-8286, USA. Tel.: +1-203-432-4332; fax: +1-203-432-4387.

E-mail address: robert.tanner@yale.edu (R.E. Tanner).

0039-6028/01/$ - see front matter
PII: S0039-6028(01)01032-9

[1]. Nickel dispersed on the surface of crystalline titanium dioxide (a mixture of anatase and rutile) has been shown to exhibit enhanced catalytic activity compared to Ni powder or Ni supported on SiO_2, Al_2O_3 or graphite. What is more, such supported Ni/TiO_2 was found to have a greater resistance towards carbon contamination and Ni sintering (agglomeration) [2]. Supported metal-on-oxide (M/O) catalysts of this type are well known as catalysts for selective oxidation. Many commercial oxidation systems rely on highly dispersed noble metals (e.g., Pt, Pd) on a high-surface-area oxide powder such as alumina or silica. These are expensive to produce and have a lifetime limited by poisoning, so catalysts that are cheaper and harder to denature are very attractive industrial alternatives. However, there is a great need for fundamental understanding of the electronic interaction of the layer with the substrate; the thermodynamic stability of the interface; and the effects of the supports oxidation state, defect density and morphology. Experiments on the powder-based systems used in catalytic converters can be very complex and are difficult to model theoretically, so recent work has concentrated on simpler, single crystal oxide substrates such as TiO_2. Surface science investigations of small metal particles supported on oxide substrates have revealed that chemisorptive and catalytic properties may depend on particle thickness, particle shape and the condition of the substrate surface, as well as just on the diameter. Exciting research into catalytically active metal on oxide systems has recently shown that it is possible to control the shape of metal particles with almost nanoscale accuracy [3–5].

Small molecules such as oxygen [6] and carbon monoxide [7] are known to adsorb on nickel metal, and atomic resolution images of CO/Ni(111) [8] and CO/Ni(110) [9] have been published. Meanwhile, room temperature molecular adsorption of CO on Ni/TiO_2 has been detected using photoemission and electron energy loss spectroscopies (XPS, UPS and EELS) [10,11]. These results demonstrate the potential viability of the Ni/TiO_2 system as a model catalyst and its suitability for investigation in ultra-high vacuum (UHV). However, reports on the catalytic chemistry of Ni/TiO_2 vastly outweigh detailed surface analysis, and the latter corpus of work is inconclusive. Many investigations seem contradictory when describing the growth mode and epitaxial-relation of the nickel to the $TiO_2(110)$ substrate beneath. Principally using scanning tunnelling microscopy (STM) and reflection high-energy electron diffraction (RHEED) we have therefore begun to characterise the Ni/TiO_2 system, starting with a clean, well-defined $TiO_2(110)$ surface and then depositing nickel from an electron beam evaporator. The work is reported in two sections: first a study of the evolution of the orientation-relations of Ni on TiO_2 with coverage; and in the second part, the effect of heat treatment and role of oxygen on the morphology and orientation of the nickel on the $TiO_2(110)$ surface.

1.1. Growth mode and orientation relations of metals on $TiO_2(110)$

Awareness of the importance of thin metal layers on oxide surfaces is reflected in the recent increase in research carried out on such systems. Good reviews are provided in Refs. [5,12,13], the last of which concentrates on metal deposition onto TiO_2. Crystalline overlayers on crystalline substrates tend to grow following a preferred "mode" and may exhibit a preferred orientation (epitaxy). In the case where there is full registry of the overlayer atoms with substrate atoms, the epitaxial overlayer is said to be "coherent", "pseudomorphic" or "commensurate" with the substrate. The energy of the M/O interface is reduced through elastic straining of the film, and even when there is limited coherency of the overlayer a preferred epitaxial orientation may be observed. Broadly speaking, metal (m) overlayer growth on an oxide surface (o) in vacuum (v) proceeds by one of three different modes. More "reactive" metals including alkali and alkaline earth metals and metals left of iron in the periodic table have low metal/oxide interface energies, $\gamma_{m/o}$, and $\gamma_{o/v} \geqslant \gamma_{m/v} + \gamma_{m/o}$. Metal overlayers deposited on the TiO_2 surface grow initially flat "wetting layers", then continue in a layer-by-layer fashion (Frank–van der Merwe, F–M) or as three-dimensional (3D) islands (Stranski–Krastanov, S–K). Strong interaction accompanied by electronic

charge transfer from the metal to TiO_2 has been demonstrated. Weaker layer–substrate interactions are observed for less ''reactive'' metals such as noble metals, nickel and copper. Here the interface energy is high, $\gamma_{o/v} < \gamma_{m/v} + \gamma_{m/o}$, and the overlayers form via agglomeration in 3D islands during Volmer–Weber (V–W) or occasionally S–K growth. The ''reactivity'' of the metal is closely related to the heat of formation of the oxide [14], and it is expected that metals such as nickel and copper would interact very little with the substrate, their oxides having heats of formation less than half of the value quoted for TiO_2 [15]. However, it was noticed at least twenty years ago that the behaviour of nickel on TiO_2 might be more complicated than this reactivity model suggested. Kao et al.'s low energy electron diffraction (LEED) investigations showed the Ni overlayer structure on TiO_2 ''depends markedly on the Ni coverage and annealing temperature'' [16]. In two other studies, strong interfacial Ni–O bonding was suggested as the cause of S–K growth of Ni/TiO_2(110) [17,18]. However, this was not confirmed using a real-space imaging technique such as STM, and the epitaxial orientations of both Cu/TiO_2(110) and Ni/TiO_2(110) are far from unanimous. This has motivated us to study the growth of nickel on single-crystal rutile TiO_2. Our initial investigations concerned the characterisation of the bare TiO_2 (110) substrate [19]. We show here that the growth mode of nickel on the TiO_2(110) surface is of 3D (V–W) type, whereby 3D Ni islands form on the TiO_2 surface. Small equiaxed nanocrystals initially exhibit random orientation, but with increasing coverage their orientation evolves so that the epitaxial-relation $(110)_{Ni}\|(110)_{TiO_2}$, $[\bar{1}10]_{Ni}\|[001]_{TiO_2}$ is established. This behaviour is observed at temperatures between room temperature and 500 K.

1.2. The effect of heat treatment, oxidation and reduction on the metal-on-oxide systems

Heating deactivates many metal-on-oxide (M/O) catalysts; in particular almost complete suppression of CO and H_2 chemisorption has been observed when metal/titania systems are subjected to high temperature reduction (e.g., annealing in H_2, or above ~725 K in UHV); yet at the same time the activity for catalysing CO hydrogenation may be enhanced [20]. Reduced M/TiO_2 systems are also reported to exhibit markedly modified catalytic behaviour in hydrogenolysis and Fischer–Tropsch synthesis [21,22]. This phenomenon has been christened the ''strong metal–support interaction'' (SMSI) and has been observed for dispersed noble metals and most group VIII metals (Ru, Rh, Pd, Os, Ir, Pt, Ni) supported on TiO_2 substrates, and is also seen for other reducible oxide substrates (Ta_2O_5, V_2O_3, MnO, Nb_2O_5) [23,24].

Metal–substrate charge transfer is insufficient to cause the suppression of CO chemisorption [25–27]; it is now known that the SMSI state is a solid-state chemical phenomenon, in which suboxide particles (''moieties'') diffuse onto the metal surface. This has been observed directly in HREM of Rh/TiO_2 [28], and in STM TiO_x has recently been imaged atop annealed Pt/TiO_2 [29]. The moieties are believed to physically block the active sites on the metal particles. For certain catalytic reactions, this catastrophic metal ''decoration'' or ''encapsulation'' leads to poisoning of the catalyst. Poisoning remains a critical and limiting problem in catalyst technology. On the other hand, since the ''poisoned'' catalyst is active for certain other reactions, it seems incongruous that more work has not focused on the Ni/TiO_2 system.

In this study, we reveal that the oxidation/reduction environment of Ni/TiO_2 induces dramatic morphological and electronic changes to the surface layers. Ni clusters annealed in UHV coarsened up to ~880 K for the coverage studied, but after this temperature the metal clusters did not grow any further. Throughout the process, the clusters maintained their orientation-relation with the substrate $(110)_{Ni}\|(110)_{TiO_2}$. The crystallography and morphology of the surface layer were altered when the samples were oxidised in air. NiO formation is inferred from the change in lattice parameter and overlayer orientation. Vacuum annealing did not restore the oxidised samples to their initial orientation, although crystals of Ni seem to be at least partially recovered.

2. Experimental details

The experimental apparatus consists of two UHV chambers pumped to a base pressure of $\sim 10^{-8}$ Pa. Up to three chemically etched Pt–Ir tips and three samples may be loaded through a fast-entry lock onto a carrousel in the treatment chamber. Following bake-out of the system, the tip and sample were transferred to the observation chamber, containing a commercially designed elevated-temperature STM (JEOL JSTM-4500XT) [30]. This chamber was additionally equipped with facilities for gas-source molecular beam epitaxy (MBE), mass spectrometry, metal deposition and RHEED. The sample was mounted at the geometrical centre of the chamber with the sources and probes aligned with the sample surface. In this way, in situ measurements and treatments may be carried out, in which combinations of techniques can be used simultaneously or in rapid succession without the need for sample manipulation. The preparation chamber was equipped with facilities for gas dosing, Ar^+ ion sputtering and a four-grid retarding-field analyser for rear-view LEED and Auger electron spectroscopy (AES).

Though pure stoichiometric TiO_2 is an insulating material, the introduction of point defects results in n-type semiconducting behaviour. Defects may be created by heating to $\sim$1000 K and subsequent cooling to room temperature. This technique ensures sufficient sample conductivity for STM measurements. (The enhanced conductivity was recently confirmed as a result principally of interstitial titanium atoms rather than oxygen vacancies as commonly quoted [31].) In this work, the single crystal TiO_2(110) wafers (Pi-KEM, Surrey, UK) were cut into pieces measuring $1 \times 2 \times 7$ mm^3 and were mounted on top of a resistively heated Si(111) wafer. High temperature reduction (typically 1100 K, 20 h) turned the samples from opaque yellow to light blue in colour. The surfaces of the samples were cleaned of debris and impurity atoms by Ar^+ ion bombardment (typically 15 min, 500 eV, drain current $\sim$5 μA). Sputter damage was removed by vacuum annealing at $\sim$1100 K for 25–35 min, resulting in a clean, planar, ordered surface, determined by AES, LEED and RHEED. An optical pyrometer was used to determine the temperature.

Nickel was deposited at 45° to the specimen from a commercial, water cooled, electron beam metal evaporator (Oxford Applied Research, model EGN4). A constant metal deposition rate was ensured via a charged-flux monitor in the e-beam evaporator. The evolution in surface crystallography with nickel coverage was monitored in real time with RHEED at growth temperatures between 295 and 495 K. Azimuthal rotation of the sample stage between 0° and 45° permitted investigation of a range of diffraction angles and hence identification of Ni growth-orientation. Two sets of samples were prepared, cut with their long side parallel to either the $[001]_{TiO_2}$ or the $[1\bar{1}0]_{TiO_2}$ direction. This allowed investigation of the full range of diffraction angles, including orthogonal TiO_2 [001] and [1$\bar{1}$0] azimuths. Three-index notation will be used for all features in the RHEED patterns, even for the two-dimensional (2D) diffracted beams, in the interest of consistency with later stages of Ni growth where 3D transmission patterns evolve.

The Pt–Ir STM tip was retracted during deposition to avoid shadowing of the specimen surface. To correlate the real-space information with changes in the diffraction pattern, the deposition was occasionally stopped to approach the tip, and constant current, empty states images were acquired with the tip held at ground potential and the sample biased. A voltage offset was entered into the STM software to account for the role of the resistively heated silicon as a potential divider.

The size distribution of Ni clusters on titania was systematically studied as a function of anneal temperature, monitored by an infrared pyrometer. Approximately 50 monolayers (ML) Ni was evaporated onto clean TiO_2(110)-(1 × 1). Empty states STM images were acquired at maximum scan range (200×200 nm^2) to provide sufficient data for statistical treatment at each anneal temperature. The STM was operated near maximum sample bias with a small tunnelling current, and extremely slow scan rate (6 min per image), so that interactions of the tip with the substrate were minimised. This maximised the tip–sample separation and allowed the *z*-piezo time to retract up to

40 nm to surmount the largest cluster apices. Images containing abrupt changes in resolution or other tip-related change were discarded and not included in the statistics presented.

In a separate experiment, the effect of oxidation/reduction treatment on Ni/TiO_2(110) systems was studied with STM and RHEED. The clean TiO_2 substrate was dosed with Ni and oxidised by exposure to air. Following scanning electron microscope (SEM) analysis, the sample was kept in air, and was replaced in UHV some 1400 h later. Surface evolution during annealing was investigated by real-time RHEED.

3. Evolution of orientation-relations with coverage

3.1. Low coverage studies and the growth mode of Ni on TiO_2(110)

The image in Fig. 1 is a constant current topograph of the TiO_2(110)-p(1 × 1) surface following exposure to Ni at 375 K. The STM image confirms that the streaking in LEED and RHEED patterns (both before and after Ni deposition) is caused by the high density of steps along $[1\bar{1}1]_{TiO_2}$ and $[\bar{1}11]_{TiO_2}$ directions. This is a result of the sputtering process and moderate anneal conditions used to prevent excessive reduction of the TiO_2 surface (and formation of a (1 × 2) reconstruction). However, no change in the LEED and RHEED patterns was detectable following Ni deposition. RHEED is therefore insensitive to this low coverage of metal, and the unchanged LEED pattern is in agreement with a previous report, wherein LEED images from the overlayer were seen only after about 4 ML Ni [32]. A low tunnelling bias ($V_s = +0.21$ V) was used to enhance the bright features in the $[001]_{TiO_2}$ direction. These are typical of the (1 × 1) terminated TiO_2(110) surface and are attributed to rows of under-coordinated in-plane Ti atoms separated by one unit cell (0.650 nm) in the $[\bar{1}10]_{TiO_2}$ direction [19].

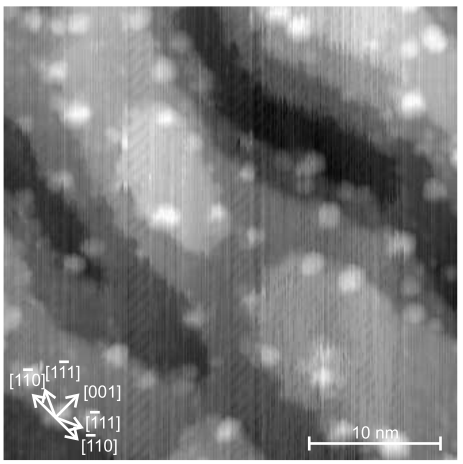

Fig. 1. At low sample bias, nickel nanoislands are seen on a TiO_2(110)-p(1 × 1) terrace resolved atomically in the $[\bar{1}10]$ direction. The islands have a strong tendency to cluster at step edges. Vertical streaking is caused by instrumental noise. $V_s = +0.21$ V, $I_t = 0.12$ nA, $T = 375$ K.

The STM image shows a large number of white features, previously absent, which we infer as a result of Ni deposition. The bare TiO_2(110)-p(1 × 1) terminated substrate is visible simultaneously with the clusters, consistent with a weak interaction between Ni–TiO_2 compared to Ni–Ni. It also implies unambiguous 3D or V–W growth, and not S–K as observed in one previous study [17], and deduced from simulations [32]. Factors that determine the growth mode include surface stoichiometry, Ni flux and temperature. In this study, the surfaces ranged from low-defect, stepped TiO_2(110) (Fig. 1) to slightly reduced (determined by the presence of white strings of sub-oxide on the terraces). However, the effect of mild surface reduction on the growth mode may be negligible: no effect was seen for Cu grown on sputtered TiO_{2-x}(110) versus TiO_2(110)-(1 × 1) samples [33]. The weak influence of surface defect density on nucleation behaviour is consistent with the weak interaction between metal overlayer film and TiO_2 substrate, and the low activation barrier for diffusion [34]. Similar behaviour is anticipated for Ni/TiO_2.

The clusters of Ni atoms in Fig. 1 and other similar STM images appear preferentially at step edges. This behaviour is attributed to the defects attracting adatoms and acting as nucleation sites, since the diffusing adatoms have a longer residence time and therefore a higher probability of meeting at such stable sites. It is impossible to state unambiguously whether the Ni clusters have nucleated at

lower or upper step edges: many appear to straddle the step. This was also observed for $Cu/TiO_2(110)$ [34], where the Cu clusters were located at lower steps, spilling onto upper terraces. In contrast, the Ni islands in Fig. 1 appear to prefer locations atop steps, even though it is impossible to rule out that the initial nucleation events occur at the lower step edge. The alternative possibility – that the nucleation event occurs at the upper step edge – may occur if under-coordinated titanium and oxygen atoms at these locations act as preferred nucleation sites due to their modified electronic properties. Alternatively, changes in substrate geometry at steps (relaxation) could create a better epitaxial match for the clusters, allowing Ni islands with a low strain energy to form.

The nickel islands have a typical diameter of ~1.6 nm. Line-scans across the clusters reveal their shape to be domes with a contact angle of ~33°. Using the definition of 1 ML from the literature [16,35], a maximum 2D coverage of $\sim 2 \times 10^{14}$ atoms cm^{-2}, or 0.2 ML is deduced. This estimation is reasonable, since the ratio of covered substrate area to bare TiO_2 area is ~1/10 and the islands are more than one atom high. Hence the deposition rate is estimated at 0.015 ML s^{-1} for the e-beam flux employed, in agreement with sub-monolayer calibration measurements at higher flux.

3.2. Determination of the orientation-relations for $Ni/TiO_2(110)$ and island morphology

Several studies in the literature have reported conflicting growth orientations of nickel on rutile $TiO_2(110)$. Low Miller index epitaxial-relations of small fcc metal clusters are visualised in Fig. 2, whilst Table 1 summarises the epitaxial mismatch values for coherent growth of Ni in various orientations on $TiO_2(110)$. Each column represents a different Miller-indexed Ni plane lying parallel to

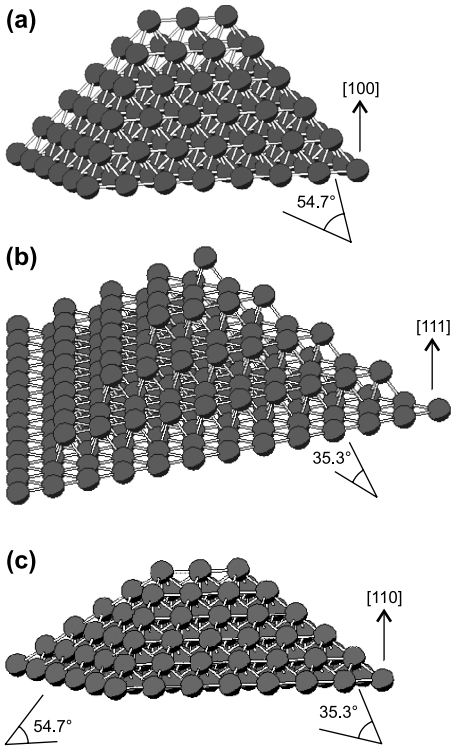

Fig. 2. Schematic illustration of small crystallites of fcc nickel with different orientations. (a) $(001)_{Ni}\|(110)_{TiO_2}$. The crystallite is depicted with {111} faces uppermost. The angle between the substrate and facets is 54.7°. (b) The hexagonal axis of $(111)_{Ni}\|(110)_{TiO_2}$. The stepped structure consists of {110}-type facets inclined at 35.3° to the substrate. (c) $(110)_{Ni}\|(110)_{TiO_2}$. The {111}-type facets on the long faces are inclined at 35.3°, whilst the {100} faces at the ends are inclined at 45°. Nearest neighbours are connected along ⟨110⟩ directions in all diagrams.

Table 1
Orientation relations and mismatch values for coherent, epitaxial Ni(*h k l*)/TiO_2(110). The coincidence, n_x, represents the number of Ni unit cells along direction x that lead to the mismatch value ε_x

	Ni(001)	Ni(001)	Ni(111)	Ni(131)	Ni(110)
Direction 1$\|\|TiO_2$[001]	Ni[100]	Ni[1$\bar{1}$0]	Ni[10$\bar{1}$]	Ni[10$\bar{1}$]	Ni[$\bar{1}$10]
Coincidence$\|\|TiO_2$[001], n_1	1	1	1	1	1
Mismatch$\|\|TiO_2$[001], ε_1	+19.0%	−15.8%	−15.8%	−15.8%	−15.8%
Direction 2$\|\|TiO_2$[1$\bar{1}$0]	Ni[010]	Ni[110]	Ni[$\bar{1}$2$\bar{1}$]	Ni[$\bar{3}$2$\bar{3}$]	Ni[001]
Coincidence$\|\|TiO_2$[1$\bar{1}$0], n_2	2	3	1	1	2
Mismatch$\|\|TiO_2$[1$\bar{1}$0], ε_2	+8.5%	+15.1%	−33.6%	+27.2%	+8.5%

the TiO_2(110) surface. The first and fourth rows show the Ni surface unit cell vectors lying parallel to $[001]_{TiO_2}$ and $[1\bar{1}0]_{TiO_2}$, respectively. The second and fifth rows give n_x, the number of d_{hkl} spacings in direction x, where $n_x d_{hkl}$ were used to calculate the mismatch values in rows three and six. The values of mismatch shown in the Table are high so fully coherent growth is not anticipated. However, reports of epitaxially oriented growth make the consideration of surface-induced strain important and therefore warrant the inclusion of the Table.

The following orientations of nickel have been reported growing parallel to the TiO_2(110) plane: Ni(100) [17], Ni(111) [17,36], Ni(111) and Ni(131) [32]. Recent cross-sectional TEM data for copper deposited onto TiO_2(110) at 475 K [37] revealed Cu(110) oriented islands, in contrast to previous work where Cu(111) was seen [14,33,38–46]. Possible representations of these nanocrystals are shown in Fig. 2.

RHEED patterns and STM images of a clean TiO_2(110) surface and after various deposition times are presented in Fig. 3. The first and last columns contain [001] and $[1\bar{1}0]$ RHEED patterns, and the middle column contains the corresponding STM images. Each row corresponds to a different

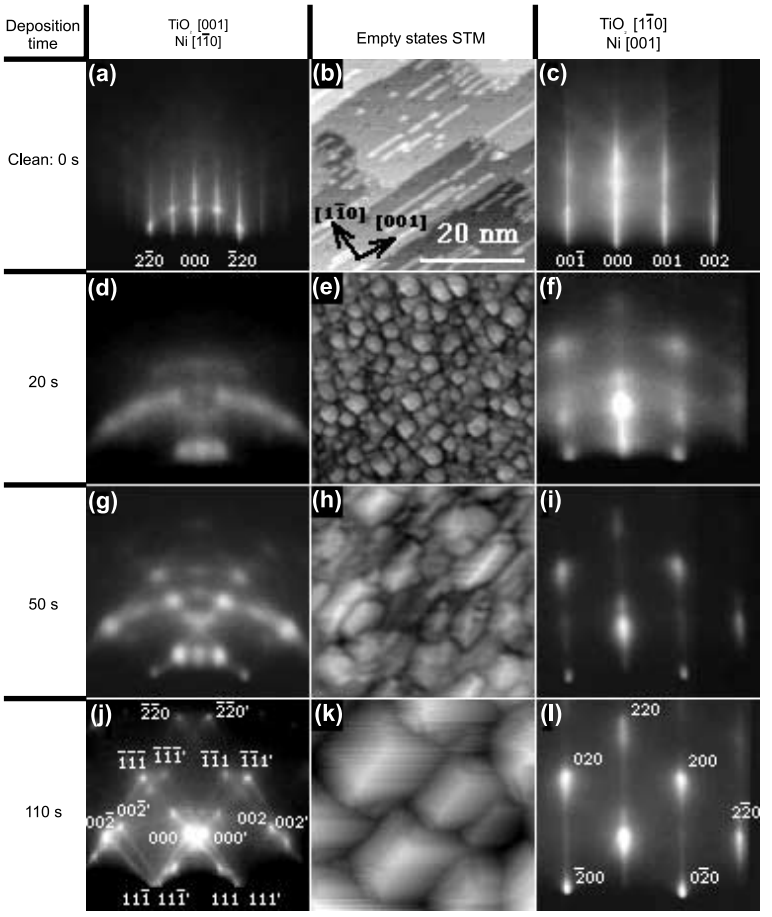

Fig. 3. Evolution of STM and RHEED images of the TiO_2(110) surface as a function of nickel coverage. (a)–(c) Bare TiO_2(110); (d)–(f) Ni deposition for 20 s; (g)–(i) 50 s; and (j)–(l) 110 s. The first column shows 12 kV RHEED patterns in the TiO_2[001] azimuth. The second column is constant current empty states STM images of the evolving surface. The third column shows 12 kV RHEED patterns in the $TiO_2[1\bar{1}0]$ azimuth. The coverage was not calibrated but is estimated to be about 1 ML after 20 s.

exposure. [001] and [1$\bar{1}$0] RHEED patterns from the TiO_2 surface prior to deposition are shown in Fig. 3(a) and (c), respectively. An STM image of the surface is shown in Fig. 3(b). The initial surface is 2D, though rather rough on the atomic scale. This roughness, due to the short terrace size and thus high density of steps, is manifested in diffraction patterns in the form of continuous streaks (Fig. 3(a) and (c)).

The evolution of the RHEED patterns with Ni-deposition time and the corresponding STM images are shown in Fig. 3(d)–(l). The Ni deposition rate was determined from sub-monolayer calibration experiments and was estimated as equivalent to the completion of 1 ML after 20 s. Within a few seconds of opening the evaporator shutter, the diffraction patterns in both $[001]_{TiO_2}$ and $[1\bar{1}0]_{TiO_2}$ crystallographic directions underwent a drastic 2D-to-3D change, confirming the earlier assignment of 3D (V–W) growth mode, from even the earliest stages. In the low-coverage images of Figs. 1 and 3(e), it could be argued that the development of 3D clusters is promoted by the substrate heating ($\sim$100 K above room temperature). However, during room temperature (RT) studies, we observed no RHEED intensity modulations corresponding to layer-by-layer growth, therefore we conclude that V–W growth of faceted clusters occurs at all temperatures between 295 and 495 K. The STM image in Fig. 3(e) displays a dense array of tiny equiaxed crystallites, 4–5 nm in diameter, shown after 20 s deposition. RHEED patterns from this surface, Fig. 3(d) and (f), exhibit diffused rings of intensity, so-called "Debye rings", originating from rotation of interplanar spacings in randomly oriented crystallites. However with increasing deposition time, i.e., increasing Ni-coverage, the size and the shape of individual crystallites changes, as can be seen in Fig. 3(h). The principal change with increasing crystallite volume is an elongation of the shape, and development of distinct crystallographic facets. Corresponding diffraction patterns, Fig. 3(g) and (i), exhibit a shift from polycrystalline to a strong preferred orientation, as can be judged from intensity pumping from the diffused rings into the spots. This trend continues, and after two minutes of deposition the well-defined nanocrystals shown in Fig. 3(k) exhibit monocrystalline diffraction patterns (Fig. 3(j) and (l)). These patterns do not change, even if more Ni is deposited or if annealed at elevated temperatures for prolonged periods of time, even though further nanocrystal growth is observed, as discussed in the second section of this paper.

The monocrystalline diffraction patterns in Fig. 3(j) and (l) are consistent with respectively $\langle 110\rangle$ and $\langle 001\rangle$ Ni transmission patterns or "zone-axes" in TEM terminology. Knowing these zones were obtained with the RHEED beam parallel to the [001] and [$\bar{1}$10] TiO_2 directions, respectively, the patterns are sufficient to define the orientation-relation with the substrate as $\{110\}_{Ni}\|(110)_{TiO_2}$, $\langle 110\rangle_{Ni}\|[001]_{TiO_2}$ and $\langle 001\rangle_{Ni}\|[\bar{1}10]_{TiO_2}$. Fig. 4 is a representation of the reciprocal space associated with the sample surface, calculated using the reciprocity definitions, and relations between the reciprocal space vectors and the geometry of RHEED apparatus. The RHEED patterns from different azimuths are superimposed at the appropriate rotations. The two additional zones at 35° and 45° rotations (Fig. 4(f) and (g)), confirm unambiguously our assignment of orientation-relation. Three TiO_2 Laue zones are seen upon 35°-rotation, where all the reflections belong to the $TiO_2[3\bar{3}2]$ pattern, and upon 45°-rotation the Ni$\langle 112\rangle$-type pattern is observed, in spite of a 9° deviation from the real [$\bar{1}1\bar{2}$] zone at 54°. The match is excellent between the location of reflections in the experimental RHEED patterns and calculated reciprocal lattice points.

In addition to the evolution of the orientation of the nanocrystals, their shape also changes with deposition time. While initially equiaxed and randomly oriented, the Ni crystallites undergo a distinct shape transition as their size increases, turning into elongated, faceted nanocrystals. Viewed from above, the Ni crystallites resemble an array of roofs, and hence are known as "hut-clusters". Facet angle measurements from lines-cans through STM images (e.g., Fig. 3(k)) and streak analysis in RHEED transmission patterns (e.g., Fig. 3(j) and (l)) indicate that the long facets are inclined at about 35° to the surface and are of $\{111\}$ type, and the short ones are possibly of $\{100\}$ type. This is also in accord with the shapes

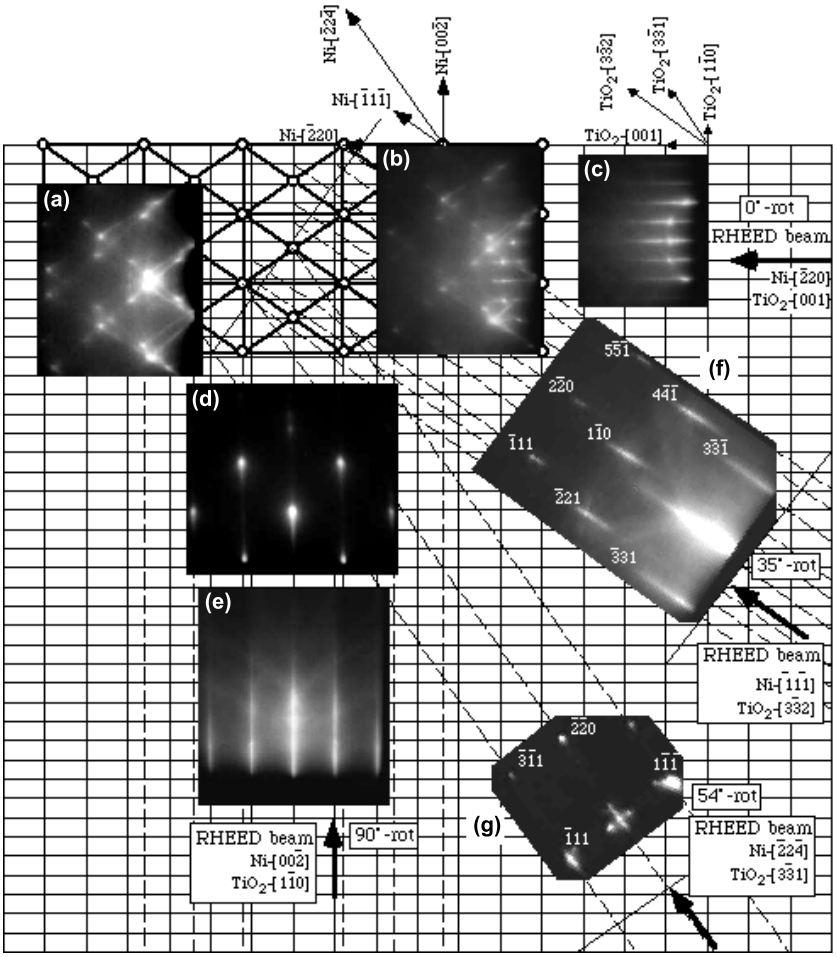

Fig. 4. (110)-section through 3D reciprocal space of Ni (thick, continuous lines and open circles) superimposed onto a $(1\bar{1}0)$ section of the TiO_2 reciprocal lattice (thin, continuous lines). The calculation is for 12 kV and 23 cm sample-screen distance. RHEED patterns from four different azimuthal directions show reflections from (a), (d), (g) the Ni film; (b) Ni film and substrate; (c), (e), (f) substrate alone.

in Fig. 2, proposed on the basis of the smaller surface energy of low Miller index planes. Previous studies of the shape of low-reactivity metal islands on oxide surfaces revealed flat-topped clusters for sub-monolayer $Pt/TiO_2(110)$ [29], $Cu/TiO_2(110)$ [34] and Pd/Al_2O_3 [47]. Although the discrepancy in behaviour may be due to higher coverage or deposition temperatures, further investigations indicated formation of 3D clusters even from the earliest stages of room temperature growth. Similar faceted crystallites were observed for comparable coverages of Cu/TiO_2 deposited at 475 K [37]. In this Cu/TiO_2 study, (110)-oriented overlayers were also observed. The steep facet angles and possibly different parameters required for STM imaging of metals meant that we were unable to image atomic-scale features on the Ni surfaces. Thus we were unable to determine whether the Ni crystallites were encapsulated with TiO_x, as was revealed on flat-topped Pt clusters [29].

The Ni $[1\bar{1}0]$ transmission pattern in RHEED reveals the presence of two crystalline orientations of the Ni, with a relative tilt of $\sim 5°$ (Figs. 3(j) and 4(a)). In Fig. 3(j), the second set of diffraction

spots is indexed with dashes. Multiple orientations for metal layers on oxides have been observed for room temperature deposition of Ni onto MgO-(002)-(1 × 1) [48], and two orientations were reported for Pt and Cu(111) overlayers on TiO_2 (110). These were interpreted as fcc stacking faults in Pt and Cu [41,49]. Previous LEED studies of Ni/TiO_2(110) led to the assignment of Ni(111) islands and Ni(131) islands tilted by 27° [32]. The epitaxial match with the substrate for these orientations is very poor however (see Table 1) and the epitaxial-relation was deduced computationally starting from the assumption of Ni(111) growth. In the present work the RHEED patterns indicate tilted Ni(110) growth, although the origin of the double spots is unclear. They may arise from growth defects (such as twins) or may reflect the layer's attempt to form registry with the substrate. Although Ni was deposited at elevated temperature, and the later RHEED patterns (Fig. 3(j) and (l)) show measured lattice constants closer to bulk Ni than TiO_2, nevertheless at lower coverages some quasi-registry of every other Ni atom can be preserved along $[001]_{TiO_2}$ resulting in a lower strain along $[1\bar{1}0]_{TiO_2}$ than for other Ni orientations (Table 1). The average mismatch in the two perpendicular directions is minimised for this orientation, so it would seem surface Ni mobility is sufficient to allow the crystallites to grow with low strain. An "areal mismatch" may be defined as:

$$\varepsilon_{xy} = \frac{d^{Ni}_{1\bar{1}0} d^{Ni}_{00\bar{2}} - d^{TiO_2}_{00\bar{1}} d^{TiO_2}_{1\bar{1}0}}{d^{TiO_2}_{00\bar{1}} d^{TiO_2}_{1\bar{1}0}} = \frac{0.249\ \text{nm}\ (2 \times 0.352\ \text{nm}) - 0.296 \times 0.650\ \text{nm}^2}{0.296 \times 0.650\ \text{nm}^2} = -8.9\%.$$

4. The effect of heat treatment and role of oxygen

4.1. High coverage: temperature dependent shape evolution

Fig. 5 shows how the size of Ni clusters on the TiO_2(110) surface varies as a function of anneal temperature. Following deposition of ~50 ML nickel onto clean TiO_2(110)-(1 × 1), elevated temperature STM images were used to monitor the changing size distribution of the Ni clusters. In the left-hand column are representative STM images at different stages of the annealing process, showing how the Ni islands maintain their "hut-cluster" shape. The right-hand column is a series of frequency distributions for the average lateral island size, defined as the arithmetic mean of the base length along the substrate $[001]_{TiO_2}$ and $[\bar{1}10]_{TiO_2}$ directions [50,51]. The bin size was set at 7 nm average lateral size, since the error associated with each set of data is approximately the standard

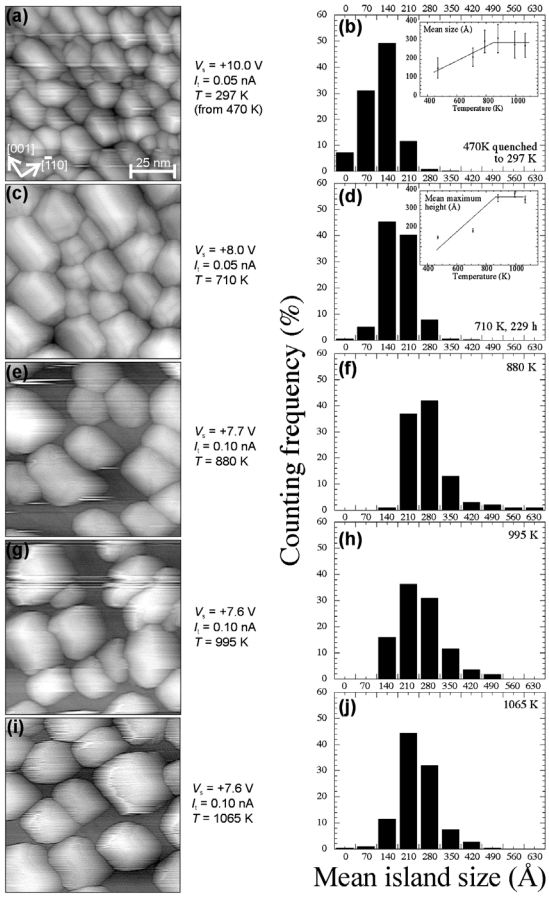

Fig. 5. Typical elevated-temperature STM images (left-hand column) and size distributions (right-hand column) for Ni/TiO_2(110) at different anneal temperatures. (a), (b) 470 K quenched to 295 K (RT), with mean size versus temperature (inset); (c), (d) 710 K, mean maximum height versus temperature (inset); (e), (f) 880 K; (g), (h) 995 K and (i), (j) 1065 K.

deviation for Gaussian spread. The figure indicates that clusters coarsen with annealing. The average lateral size, plotted in the inset of Fig. 5(b), shifts to higher values with increasing temperature for the first three temperatures. Above ~880 K it is constant at ~28 nm for all temperatures. Similar behaviour is observed for average maximum cluster height versus temperature, inset Fig. 5(d). The height increases from 15 nm immediately after quenching, to ~36 nm at 880 K, and is approximately constant for higher temperatures. Coarsening is evidence for the natural self-organisation of the surface adatoms, where the driving force is the reduction in surface energy of the islands. The equilibrium state, when all the deposited Ni is in one large island, was not attained here. However, the final state may not be attained if the island-ripening process is opposed by diffusion or interface mass-transfer barriers.

The mechanism by which clusters on surfaces evolve and coarsen is modelled in the Lifschitz, Slyozov and Wagner (LSW) theory [52,53]. This analytical mean-field theory was extended to surfaces by Chakravery [54,55] and predicts distributions of 3D island sizes that are negatively skewed when dominated by ripening mechanisms. Such distributions have been observed for Ga/GaAs(001) and Ge/Si(100) [56–58]. Positively skewed (log normal) or symmetrical (Gaussian) distributions have been attributed to coalescence-dominated behaviour. A rigorous treatment of the data following the LSW formalism cannot be applied here, since the cluster–cluster interactions are non-negligible for high cluster density. However, some qualitative trends may be inferred from Fig. 5. Most of the size distribution functions in the right-hand column are asymmetric. At the growth temperature (subsequently quenched to RT), the distribution is slightly negatively skewed, whilst at temperatures between 710 and 1065 K it is positively skewed. Expansion of the sample prohibited STM investigation during temperature ramping. Images showed immobile clusters at fixed temperature, indicating that dynamic coalescence processes were not responsible for changes in island shape at constant temperature. The flux of Ni to the surface during annealing was zero (neglecting diffusion into and out of the substrate) so the data indicate that the shape evolution is most likely to occur via static coalescence (reorganisation) of touching clusters. Above ~880 K the cluster size is constant with increasing temperature and it would seem that this process is almost complete. The empty, denuded zones around large clusters (Fig. 5(e), (g) and (i)) imply a certain degree of Ostwald ripening. We believe this indicates that both mechanisms are active at different stages.

4.2. LEED of annealed Ni/TiO_2(110)

During annealing of ~50 ML Ni on TiO_2(110), the LEED pattern from the surface revealed new features that were absent from LEED patterns at low Ni coverage. The extra features appear due to diffraction from the Ni islands, as previously reported for coverages of $\theta_{Ni} > 4$ ML [32]. The LEED images of Ni/TiO_2(110) annealed to 710 K, Fig. 6, were taken from the Ni/TiO_2 sample of Fig. 5(c) and (d). A smaller LEED image from a typical, clean surface is presented in Fig. 6(a) for comparison. In the right hand column each of the spots from the rectangular TiO_2(110) mesh is indicated with a black circle, including the supposed position of spots masked by the electron gun. In addition to the TiO_2 mesh, additional features may be seen in Fig. 6(b) and (c) that are due to the Ni overlayer. Some are indicated with small arrows. The Ni pattern is symmetrical with respect to the [001] axis, though no clear 2D mesh is discernible.

The parallel sets of Ni spots and streaks are indicated by arrows and are more widely spaced than the spots of the TiO_2 reciprocal lattice along $[001]_{TiO_2}$. The separation of the Ni features corresponds to a periodicity of 0.251 ± 0.01 nm, consistent with the Ni–Ni separation along $\langle 110 \rangle_{Ni}$ directions. To define the layer orientation unambiguously requires a second direction of periodic spots, not present in Fig. 6(b) and (c). The 0.25 nm repeat is wholly consistent with RHEED, in which a Ni$\langle 1\bar{1}0 \rangle$ zone axis pattern parallel to the substrate $[001]_{TiO_2}$ direction was observed.

The Ni spots move rapidly across the pattern along $[1\bar{1}0]_{TiO_2}$ and $[001]_{TiO_2}$ directions as the electron energy is changed. In contrast, substrate diffraction spots move slowly outward, following a

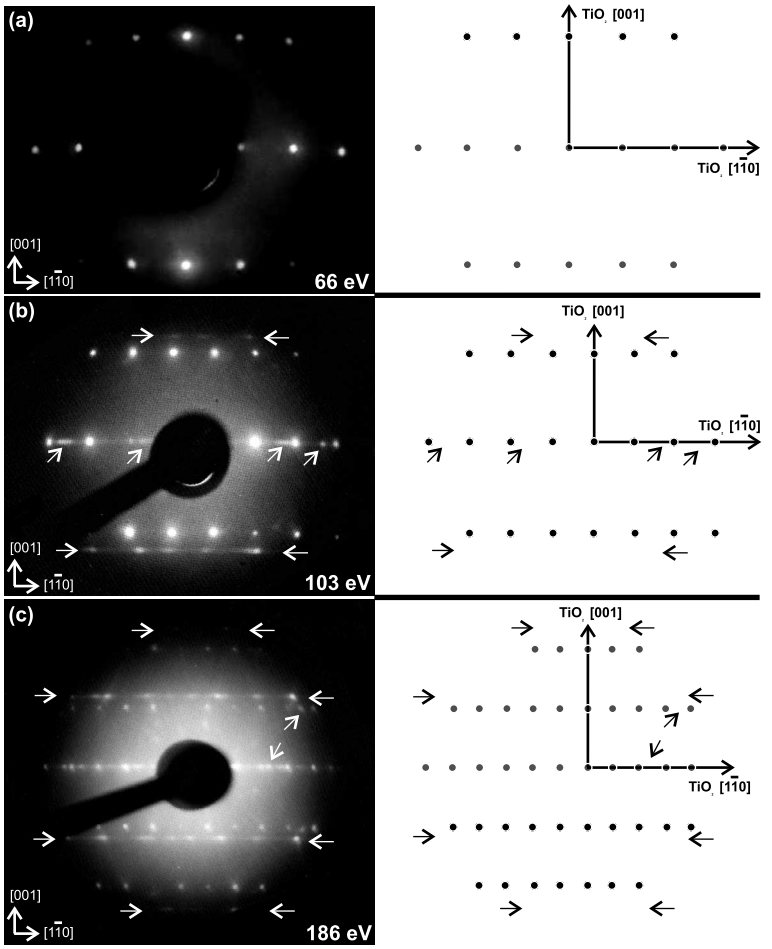

Fig. 6. LEED patterns at different primary electron energies from the $TiO_2(110)$ surface. (a) A typical pattern from clean $TiO_2(110)$ before deposition. (b) and (c) LEED patterns from an annealed overlayer of approximately 50 ML Ni on $TiO_2(110)$, $T = 710$ K. To the right of each pattern, the diffraction spots from the rectangular $TiO_2(110)$ array are shown as a black circles. Some of the stronger features resulting from diffraction from the Ni clusters are indicated by arrows. The separation of the parallel lines of these Ni spots reveals a periodicity of ~0.25 nm in the [001] direction, whilst no periodicity is clear along [$\bar{1}$10].

trajectory based on Ewald sphere treatment with $(0,0)$ pattern centre. This complex behaviour of the Ni diffraction spots is indicative of faceted surfaces, in agreement with STM data. Similar LEED patterns were reported for 8 nm Ni on $TiO_2(110)$ annealed to 520 K for 7.5 min [32]. Complex spot motion was also reported in the $[\bar{1}10]_{TiO_2}$ direction, though not in $[001]_{TiO_2}$. Simulations reproduced the patterns by assuming Ni(111) and tilted Ni(111) growth. The calculated tilt angle of 27° corresponded to Ni(131) crystallites, although both Ni(131) and Ni(111) crystallites have a large associated strain (Table 1). Our RHEED studies of Ni/TiO_2 revealed Ni(110)-oriented islands composed of two crystalline regions with a relative tilt of ~5° in the Ni[1$\bar{1}$0] zone axis. The LEED pattern is consistent with this assignment, with Ni(110) periodicity revealed parallel to $[001]_{TiO_2}$. The ambiguous periodicity in the orthogonal direction may be connected to the tilt seen in RHEED, or the faceted sides of the hut-clusters. LEED is a good method of checking for

long-range order on surfaces. It is a complementary technique to STM since it averages over large areas and shows whether the real-space STM images are representative of the whole surface. However, it is less sensitive to low overlayer coverages than RHEED and is ill adapted to growth studies.

The LEED patterns reveal the same assignment of epitaxial relation as determined by RHEED.

4.3. SEM of annealed Ni/TiO_2

The annealed surface of Fig. 5(i) was also studied by scanning electron microscopy to confirm the final state of the clusters. A secondary electron image of the surface taken at 20 kV is presented in Fig. 7. In the SEM micrograph, the grey box indicates an area equivalent in size to the 100×100 nm^2 STM topographs in Fig. 5. Fig. 5 and further SEM images reveal a large variation in cluster density from one part of the sample to another, and even between 100×100 nm^2 areas. The range in cluster densities therefore stems from the chosen area on the surface and the sampling size, and affirms the need to sample from different areas for statistical purposes. Fig. 7 reveals a similar range in sizes but lower number density compared to data from STM images. This is most likely to be due to the insensitivity of SEM to smaller clusters (demonstrated for another sample in which the ~5 nm diameter clusters were not visible).

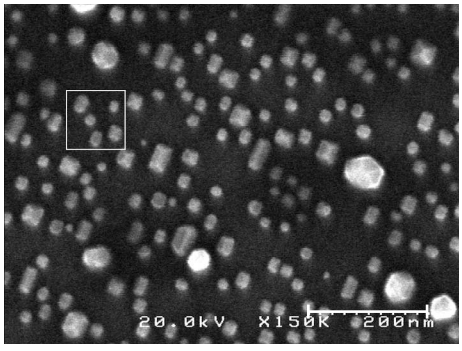

Fig. 7. Scanning electron microscope image of Ni/TiO_2(110) annealed to 1065 K. This secondary electron image at 20 kV shows "hut"-shaped crystallites on the surface. Many are of square or rectangular base area. Others are larger with hexagonal footprints and others still seem to be domes. The grey box indicates an area 100×100 nm^2, equivalent to the areas shown in the left-hand column of Fig. 5.

Hut-shaped crystallites are present that have large facets measured at $\sim 35^\circ \pm 5^\circ$. This agrees well with the earlier assignment of Ni{111}-type long facets on the basis of STM linescans, RHEED streak analysis and surface energy arguments (Fig. 2). Many of the hut-clusters have rectangular and square bases, but a proportion have developed hexagonal bases and dome-like structures. The domed structures with large heights are difficult to image in STM as the tip is forced to trace larger and larger contours over the surface. The development of these large structures was not accompanied by any modification of the RHEED pattern, indicating either that they preserve the same epitaxial relation with the substrate, or are rare and do not contribute significantly to the RHEED pattern. The new features may be formed at high temperature after the huts attain a certain critical size. Above ~880 K the growth stops (Fig. 5(b) inset and (d) inset) and a phase transformation to clusters of different geometry may occur. Large features are also seen for the Ge/Si(100) system, where a phase transformation model describes the shift from hut-clusters to domes [59,60]. For Ni/TiO_2(110) it is likely that the true transition temperature is >1000 K, since the majority of the clusters in the SEM images are still hut-shaped even after annealing to 1065 K.

Alternatively, the domes may be explained as hut-clusters that have undergone a chemical change due to exposure to air between the UHV system and the SEM. In order to investigate this hypothesis further, studies on film oxidation were carried out, as described in the next section.

4.4. Oxidation/reduction studies of $Ni/TiO_2(110)$

A clean TiO_2(110) surface (Fig. 8(a)) was dosed with 1.4 ML Ni at 495 K. Images of this surface (Fig. 8(b)) showed equiaxed crystallites, 4–5 nm in size, with a slight preferential alignment, manifested in the weak Ni⟨100⟩ transmission pattern

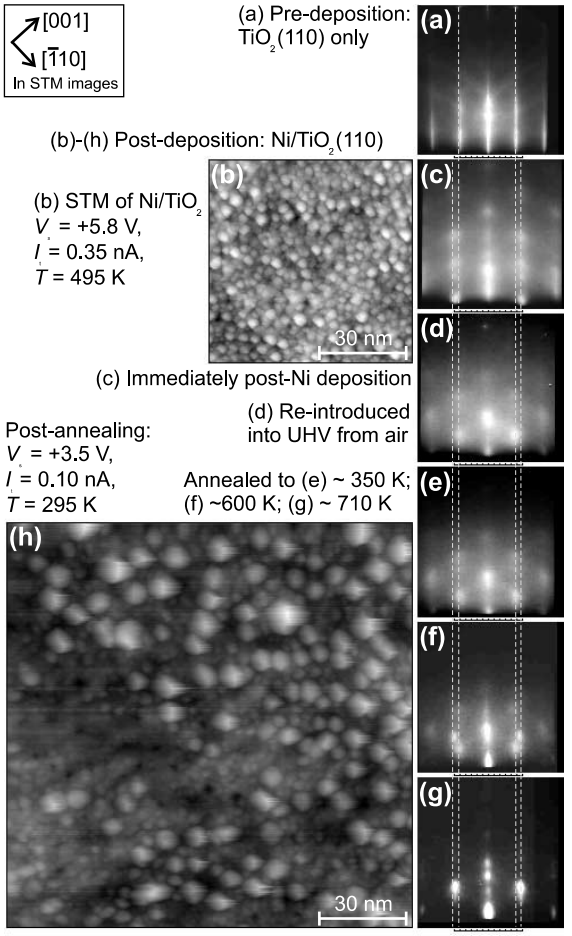

Fig. 8. Annealing low-coverage Ni/TiO_2(110). (a) Pre-deposition RHEED of bare TiO_2. Ni/TiO_2 before annealing: (b) STM image and (c) corresponding 12 kV RHEED pattern. (d)–(g) Evolution of RHEED images during annealing. (h) STM image of the surface with RHEED pattern shown in (g).

(Fig. 8(c)). The sample was exposed to air and the electron beam in the SEM and was returned to UHV some 1400 h later. The RHEED pattern unexpectedly showed a new coherent pattern in the $TiO_2[1\bar{1}0]$ azimuth (Fig. 8(d)). This arrangement of spots is characteristic of a $\langle 110\rangle$-type zone axis and was confirmed by the appearance of a $\langle 100\rangle$ zone axis pattern at 45° azimuthal rotation.

The Ni spots at the shadow edge (Fig. 8(c)) are not present after exposure to air (Fig. 8(d)) and the spots no longer lie on the outer dashed grey lines, but have moved inward. The spot periodicity is equivalent to 0.15 ± 0.01 nm along $[001]_{TiO_2}$ and 0.22 ± 0.01 nm along $[1\bar{1}0]_{TiO_2}$.

Since NiO has a rocksalt structure, the Ni–Ni (or O–O) distance in the two interpenetrating fcc lattices is 0.295 nm along $\langle 110\rangle_{NiO}$ directions. These values are in good agreement with double the measurement of the {220} periodicity in the RHEED pattern, where the (110) and $(\bar{1}\bar{1}0)$ spots are absent as one would expect for a $\langle 110\rangle$ zone axis. The perpendicular $[002]_{NiO}$ direction has a periodicity of 0.209 nm ($\frac{1}{2}a_{0,NiO}$), also in good agreement with the measurement from the RHEED pattern.

NiO formation is plausible following of exposure of the Ni overlayer to excess oxygen at atmospheric pressure. Ni oxidises easily ($\Delta H_f^\circ = 241$ kJ mol^{-1} [61]) and the lattice parameters of the 3D crystallites are consistent with the formation of NiO, epitaxially oriented so that:

$$(001)_{layer} \| (110)_{TiO_2},$$

$$[1\bar{1}0]_{layer} \| [001]_{TiO_2}, \quad [110]_{NiO} \| [1\bar{1}0]_{TiO_2}.$$

If the overlayer has been oxidised to NiO, the driving force for this orientation-relation must be the close match of the Ni–Ni (or O–O) separation in NiO (0.2954 nm) and the Ti–Ti separation in TiO_2 (0.2958 nm). The mismatch of NiO(001) with TiO_2(110) is $\varepsilon_1 = -0.15\%$, $\varepsilon_2 = -9.1\%$, implying a system with very low strain in one direction.

Heating the oxidised crystallites in UHV caused further evolution of the RHEED pattern. Between RT and 350 K the diffraction spots attributed to NiO became progressively sharper (Fig. 8(e)). At 600 K, Fig. 8(f), new diffraction spots appeared with a wider spacing that sharpened rapidly at ~615 K. Following the transformation, the pattern (Fig. 8(g)) shows a considerably reduced background intensity and a $\langle 110\rangle$ zone. The zone axis type has not changed, but there has been a contraction of the spot spacing along both directions. The periodicities of 0.13 nm for {220} spots and 0.175 nm for {200} spots correspond well with the value of $d_{220} = 0.124$ nm and $d_{002} = 0.176$ nm in Ni. This demonstrates that the overlayer has been reduced to metallic Ni. Rotation of the sample by 45° again confirmed the assignment by

revealing a ⟨001⟩ transmission pattern. The reduced crystallites are differently orientated compared to the case of Ni deposition in UHV. Here the orientation-relation is:

$$(001)_{\text{layer}} \| (110)_{TiO_2},$$

$$[1\bar{1}0]_{\text{layer}} \| [001]_{TiO_2}, \quad [110]_{Ni} \| [1\bar{1}0]_{TiO_2}.$$

For coherent growth on TiO_2(110), the mismatch values are $\varepsilon_1 = -15.8\%$, $\varepsilon_2 = +15.1\%$, so the Ni layer would be highly strained in both directions.

STM images acquired at ~720 K (Fig. 8(h)) show a dramatic change in surface morphology to a smaller number of larger islands of 8–9 nm typical lateral dimension, that have square or rectangular footprints and distinct faceted sides. Between the islands the TiO_2(110) substrate is revealed. It is impossible to estimate the volume of the Ni crystallites from the deposition flux, since the level of in-diffusion into the TiO_2 lattice is unknown. In-diffusion is reported to occur at temperatures as low as 575 K for Ni/TiO_2(110) [16] and at room temperature for Ni on defective TiO_2(110) [62] or rough TiO_2(100) surfaces [63]. Out-diffusion was observed for the samples in this study when sputter cleaning and subsequent annealing caused Ni precipitation to the surface, and formation of new islands.

In view of the large oxygen affinity of Ti with respect to Ni, the reduction of NiO may be caused by a competition between NiO and TiO_x for the oxygen in the NiO film. This elevated temperature reaction may be written $Ni^{2+} + Ti^{n+} \rightarrow Ni^0 + Ti^{4+}$, $n < 4$ [62]. TiO_x is present in the surface layers of the crystal in the form of oxygen defects, and small particles of TiO_x are known to diffuse across the surface of metals supported on TiO_2(110) [28,35]. The transformation of the film may be linked to the suppression of small molecule adsorption due to the SMSI phenomenon and it is possible that the Ni islands in the STM image of Fig. 8(h) are covered with thin TiO_x film.

To account for the different orientation of Ni after oxidation and reduction, we discount the effects of defects at the Ni/TiO_2 interface. Although step-edges are known nucleation sites for Pd, Cu and Ag on TiO_2 [3,34,64] and Pd/Al_2O_3 [47], terrace defects and surface reduction only weakly affect the behaviour of unreactive metals [33]. Instead, we believe an irreducible layer of NiO persists at the Ni/TiO_2 boundary where the annealing process does not fully reduce the NiO. In separate studies, oxidation of single crystal Ni(100) surfaces have been shown to result in the formation of a stable NiO(100) layer [65]. Vestiges of crystalline NiO are still present in the RHEED pattern of the annealed Ni/TiO_2 sample (Fig. 8(g)). We therefore attribute the anomalous Ni(001) orientation upon reduction to the stabilising effect of an interfacial NiO layer. This avoids a Ni/TiO_2 orientation with poor strain optimisation, and leads to formation of a Ni(001)/NiO(001)/TiO_2(110) system.

These results mean that the effect of exposure to air is to modify the crystallites' behaviour in response to UHV annealing and the work confirms the stability of multiple Ni orientations on TiO_2(110), suggesting that other orientations of Ni films may also be achievable under certain conditions.

5. Conclusions

It is evident from Figs. 1 and 3 that Ni does not wet the TiO_2(110) surface even at a monolayer coverage. Assuming that the previous work that indicated S–K growth at room temperature using AES [17,32] was indeed observing the same system, we prefer our interpretation, since we find STM and RHEED more appropriate for determining surface structure and topography. The data here indicate that the growth mode of Ni/TiO_2(110) at temperatures between 295 and 495 K is better described by a V–W, rather than S–K, mode, in agreement with thermodynamic expectations.

Crystalline islands of Ni(110) are formed on TiO_2(110). Previous reports of orientations with very high mismatch may be a direct consequence of the low-coverage, room-temperature conditions under which kinetically limited phases grow. In our case, the low-strain optimisation of orientation-relations can be attributed to increased surface mobility at elevated temperature, and possibly slight surface reduction.

At low coverages strained layers are formed and the lattice match for Ni(110) is better along $[001]_{TiO_2}$ and for every second Ni atom along $[1\bar{1}0]_{TiO_2}$ than for other Ni orientations. The same orientation-relation was reported recently for Cu/TiO_2(110) [37]. Both the observations of the V–W growth mode and the previously unreported orientation-relation for Ni/TiO_2 are reminiscent of discrepancies over results on Cu growth on TiO_2. Copper is another fcc metal that neighbours Ni in the periodic table and with similar heat of formation. Some authors reported the S–K growth mode for Cu/TiO_2(110), whereas others favoured V–W. There is now a general consensus that Cu films grow via the V–W mode at low coverages [14, 33,38,40–43,45,46]. In these references there is also broad agreement that the films grow in the Cu(111) orientation. In contrast and in direct agreement with the work here on Ni deposition, HREM of Cu deposited onto TiO_2(110) at 475 K revealed growth via the V–W mode and formation of Cu(110) oriented crystallites with well-defined {111}-type crystalline facets [37]. From this study, it would seem that the behaviour of RT Ni and elevated temperature Cu deposited on TiO_2(110) are similar.

When STM and electron diffraction were used to examine the effect of heat treatment on the nickel nanoisland morphology, in situ experiments showed that the orientation relation between the Ni overlayer and TiO_2(110) substrate did not change during annealing to temperatures as high as 1065 K, maintaining the orientation relation that develops during deposition: $(110)_{Ni}\|(110)_{TiO_2}$, $[\bar{1}10]_{Ni}\|[001]_{TiO_2}$. This arrangement has a low average lattice mismatch in the two orthogonal surface directions. Upon heating a 50 ML layer, the clusters coarsened up to 880 K, and their mean size reached approximately 25 nm (average of length and breadth) and ~35 nm in height, after which point the clusters did not grow any further with increased temperature. Such self-limiting growth has been discussed recently in relation to Cu deposition on TiO_2(110) [34].

RHEED patterns suggest a transformation to NiO particles upon oxidation of the Ni clusters. Crystalline particles formed that have lattice parameters consistent the formation of NiO. The crystalline overlayer was aligned so that $(001)_{layer}\|(110)_{TiO_2}$. When reduced again in UHV, the crystallites' lattice parameters returned to the value for Ni. Hut-clusters with well-defined facets were formed but the original orientation was not recovered. The new orientation of these Ni(001) clusters may be stabilised by an interfacial layer of irreducible NiO(001). These results have implications for the use of Ni on reducible substrates in supported metal catalysis, where metal/ceramic systems are used to promote selective oxidation reactions.

Acknowledgements

The authors thank Doug Perovic at the University of Toronto for the use of microscope facilities, and Dave Goddard and BNFL for the provision of a CASE studentship (RET). This work was additionally supported by EPSRC grant GR/K08161. Fig. 2 was generated with the help of BALSAC (version 2.0, K. Hermann © 1991–1996). The BALSAC software was developed by K. Hermann, Fritz-Haber-Institut Berlin, Germany.

References

[1] J.M. Thomas, W.J. Thomas, Principles and Practice of Heterogeneous Catalysis, VCH, 1997.
[2] M.A. Vannice, R.L. Garten, Metal–support effects on the activity and selectivity of Ni catalysis in CO/H_2 synthesis reactions, J. Catal. 56 (1979) 236–248.
[3] C. Xu, X. Lai, G.W. Zajak, D.W. Goodman, Scanning tunnelling microscopy studies of the TiO_2(110) surface: structure and the nucleation growth of Pd, Phys. Rev. B 56 (1997) 13464–13482.
[4] M. Frank, S. Andersson, J. Libuda, S. Stempel, A. Sandell, B. Brena, A. Giertz, P.A. Buhwiler, M. Bäumer, H.-J. Freund, Particle size dependent CO dissociation on alumina-supported Rh: a model study, Chem. Phys. Lett. 279 (1997) 92–99.
[5] C.T. Campbell, Chemisorption on metal films on oxide surfaces, Curr. Opin. Solid St. M. 3 (1998) 439–445.
[6] L. Ruan, F. Besenbacher, I. Stensgaard, E. Laegsgaard, Atom resolved discrimination of chemically different elements on metal surfaces, Phys. Rev. Lett. 70 (1993) 4079–4082.

[7] R.J. Behm, G. Ertl, V. Penka, Adlayer geometry and structural effects in the CO/Ni(110) system, Surf. Sci. 160 (1985) 387–399.
[8] P.T. Sprunger, F. Besenbacher, I. Stensgaard, STM investigation of the Ni(111)-c(4 × 2)-2CO structure, Chem. Phys. Lett. 243 (1995) 439–444.
[9] P.T. Sprunger, F. Besenbacher, I. Stensgaard, STM study of the Ni(110)-c(2 × 1)-2CO system – structure and bonding-site determination, Surf. Sci. 324 (1995) L321–L327.
[10] H. Onishi, T. Aruga, C. Egawa, Y. Iwasawa, Adsorption of CH_3OH, HCOOH and SO_2 on TiO_2(110) and stepped TiO_2(441) surfaces, Surf. Sci. 193 (1988) 33–46.
[11] M.-C. Wu, P.J. Møller, Adsorption of CO on Ni-promoted TiO_2(110), Surf. Sci. 250 (1991) 179–184.
[12] C.T. Campbell, Ultrathin metal films and particles on oxide surfaces: structural, electronic and chemisorptive properties, Surf. Sci. Rep. 27 (1997) 1–111 and references therein.
[13] U. Diebold, J.-M. Pan, T.E. Madey, Ultrathin metal film growth on TiO_2(110): an overview, Surf. Sci. 331–333 (1995) 845–854.
[14] U. Diebold, J.-M. Pan, T.E. Madey, Ultrathin metal films on TiO_2(110): metal overlayer spreading and surface reactivity, Surf. Sci. 287–288 (1993) 896–900.
[15] V.E. Henrich, P.A. Cox, The Surface Science of Metal Oxides, Cambridge University Press, Cambridge, MA, 1994.
[16] C.C. Kao, S.C. Tsai, M.K. Bahl, Y.W. Chung, W.J. Lo, Electronic properties, structure and temperature-dependent composition of nickel deposited on rutile titanium dioxide (110) surfaces, Surf. Sci. 95 (1980) 1–14.
[17] H. Onishi, T. Aruga, C. Egawa, Y. Iwasawa, Photoelectron spectroscopic study of clean and CO adsorbed Ni/TiO_2(110) interfaces, Surf. Sci. 233 (1990) 261–268.
[18] P.L. Cao, D.E. Ellis, V.P. Dravid, First-principles study of initial stage of Ni thin-film growth on a TiO_2(110) surface, J. Mater. Res. 14 (1999) 3684–3689.
[19] R.E. Tanner, M.R. Castell, G.A.D. Briggs, High resolution scanning tunnelling microscopy of the rutile TiO_2(110) surface, Surf. Sci. 412–413 (1998) 672–681.
[20] S.J. Tauster, S.C. Fung, R.L. Garten, Strong metal–support interactions: group VIII noble metals supported on TiO_2, J. Am. Chem. Soc. 100 (1978) 170–175.
[21] J.-M. Herrmann, P. Pichat, Metal–support interactions: an in situ electrical conductivity study of Pt/TiO_2 catalysts, J. Catal. 78 (1982) 425–435.
[22] T. Komaya, A.T. Bell, Z. Weng-Sieh, R. Gronsky, F. Engelke, T.S. King, M. Pruski, Effects on the structure and Fischer–Tropsch synthesis activity of Ru/TiO_2, J. Catal. 152 (1995) 350–359.
[23] S.J. Tauster, S.C. Fung, R.T.K. Baker, J.A. Horsley, Strong-interactions in supported-metal catalysts, Science 211 (1981) 1121–1125.
[24] G.L. Haller, D.E. Resasco, Metal–support interaction: group VIII metals and reducible oxides, Adv. Catal. 36 (1989) 173–235.
[25] J.A. Horsley, A molecular orbital study of strong metal–support interaction between platinum and titanium dioxide, J. Am. Chem. Soc. 101 (1979) 2870–2874.
[26] H.R. Sadeghi, V.E. Henrich, Rh on TiO_2 – model catalyst studies of the strong metal–support interaction, Appl. Surf. Sci. 19 (1984) 330–340.
[27] H.R. Sadeghi, V.E. Henrich, Electronic interactions in the rhodium/TiO_2 system, J. Catal. 109 (1988) 1–11.
[28] S. Bernal, F.J. Botana, J.J. Calvino, C. López, J.A. Pérez-Omil, J.M. Rodríguez-Izquierdo, High-resolution electron microscopy investigation of metal–support interactions in Rh/TiO_2, J. Chem. Soc. Faraday Trans. 92 (1996) 2799–2809 and references therein.
[29] O. Dulub, W. Hebenstreit, U. Diebold, Imaging cluster surfaces with atomic resolution: the strong metal–support interaction state of Pt supported on TiO_2(110), Phys. Rev. Lett. 84 (2000) 3646–3649.
[30] M.R. Castell, C. Muggelberg, G.A.D. Briggs, D.T. Goddard, Scanning tunnelling microscopy of the UO_2(111) surface, J. Vac. Sci. Technol. B 14 (1996) 966–969.
[31] M.A. Henderson, Mechanism for the bulk-assisted reoxidation of ion sputtered TiO_2 surfaces: diffusion of oxygen to the surface or titanium to the bulk?, Surf. Sci. 343 (1995) L1156–L1160.
[32] M.-C. Wu, P.J. Møller, Epitaxial growth of ultrathin Ni films on NiO(100) and TiO_2(110), Surf. Sci. 279 (1992) 23–32.
[33] U. Diebold, J.-M. Pan, T.E. Madey, Growth mode of ultrathin copper layers on TiO_2(110), Phys. Rev. B 47 (1993) 3868–3876.
[34] D.A. Chen, M.C. Bartlet, R.Q. Hwang, K.F. McCarty, Self-limiting growth of copper islands on TiO_2(110)-(1 × 1), Surf. Sci. 450 (2000) 78–97.
[35] S. Takatani, Y.W. Chung, Effect of high temperature reduction ion the surface composition of the CO chemisorption on Ni/TiO_2, Appl. Surf. Sci. 19 (1984) 341–347.
[36] S. Bourgeois, P. Le Seigneur, M. Perdereau, D. Chandesris, P. Le Fèvre, H. Magnan, A surface EXAFS study of thin nickel deposits on (110) TiO_2 surfaces, Thin Solid Films 304 (1997) 267–272.
[37] M. Wagner, O. Kienzle, D.A. Bonnell, M. Rühle, Non-stoichiometry on TiO_2(110) and Cu/TiO_2 interfaces, J. Vac. Sci. Technol. A 16 (1998) 1078–1085.
[38] P.J. Møller, M.-C. Wu, Surface geometrical structure and incommensurate growth: ultrathin Cu films on TiO_2(110), Surf. Sci. 224 (1989) 265–276.
[39] M.-C. Wu, P.J. Møller, Studies of the electronic structure of ultrathin Cu films on a TiO_2(110) surface, Surf. Sci. 224 (1989) 250–264.
[40] M.-C. Wu, P.J. Møller, Direct and substrate-phonon-assisted electronic transitions in Cu/TiO_2(110) observed by AREELS, Surf. Sci. 235 (1990) 228–234.
[41] J.-M. Pan, B.L. Maschhoff, U. Diebold, T.E. Madey, Structural study of ultrathin metal films on TiO_2 using LEED, ARXPS and MEED, Surf. Sci. 291 (1993) 381–394.

[42] A.K. See, R.A. Bartynski, Electronic properties of ultrathin Cu and Fe films on TiO_2(110) studied by photoemission and inverse photoemission, Phys. Rev. B 50 (1994) 12064–12072.
[43] P.L. Wincott, J.S.G. Irwin, G. Jones, P.J. Hardman, G. Thornton, S. Weichel, P.J. Møller, V.R. Dhanak, Angle-resolved photoemission studies of the Γ Shockley surface state on ordered Cu(111) overlayers on TiO_2(110), Surf. Sci. 377–379 (1997) 242–246.
[44] D.L. Carroll, M. Wagner, M. Rühle, D.A. Bonnell, The thermal stability of thin copper films deposited on TiO_2(110) studied by scanning tunnelling microscopy, J. Mater. Res. 12 (1997) 975–983.
[45] D.L. Carroll, M. Wagner, M. Rühle, D.A. Bonnell, Schottky-barrier formation at nanoscale metal–oxide interfaces, Phys. Rev. B 55 (1997) 9792–9799.
[46] M. Wagner, T. Wagner, D.L. Carroll, J. Marien, D.A. Bonnell, M. Rühle, Model systems for metal–ceramic interface studies, M.R.S. Bull. 22 (1997) 42–48.
[47] K. Højrup Hansen, T. Worren, S. Stempel, E. Lægsgaard, M. Bäumer, H.-J. Freund, F. Besenbacher, I. Stensgaard, Palladium nanocrystals on Al_2O_3: structure and adhesion energy, Phys. Rev. Lett. 83 (1999) 4120–4123.
[48] E.B. Svedberg, P. Sandström, J.-E. Sundgren, J.E. Greene, L.D. Madsen, Epitaxial growth of Ni on MgO(002)-(1×1): surface interaction versus multidomain strain relief, Surf. Sci. 429 (1999) 206–216.
[49] H.-P. Steinrück, F. Pesty, L. Zhang, T.E. Madey, Ultrathin films of Pt on TiO_2(110): growth and chemisorption-induced surfactant effects, Phys. Rev. B 51 (1995) 2427–2439.
[50] I. Goldfarb, P.T. Hayden, J.H.G. Owen, G.A.D. Briggs, Nucleation of "hut" pits and clusters during gas-source molecular beam epitaxy of Ge/Si(001) in in-situ scanning tunnelling microscopy, Phys. Rev. Lett. 78 (1997) 3959–3962.
[51] I. Goldfarb, G.A.D. Briggs, Reactive deposition epitaxy of $CoSi_2$ nanostructures on Si(001): nucleation and growth and evolution of dots during anneal, Phys. Rev. B 60 (1999) 4800–4809.
[52] I.M. Lifshitz, V.V. Slyozov, The kinetics of precipitation from supersaturated solid solutions, J. Phys. Chem. Solids 19 (1961) 35–50.
[53] C. Wagner, Theorie der Alterung von Niederschlagen durch Umlose (Ostwald-reifung), Z. Electrochem. 65 (1961) 581–591.
[54] B.K. Chakraverty, Grain size distribution in thin films: 1. Conservative systems, J. Phys. Chem. Solids 28 (1967) 2401–2412.
[55] B.K. Chakraverty, Grain size distribution in thin films: 2. non-conservative systems, J. Phys. Chem. Solids 28 (1967) 2413–2421.
[56] M. Zinke-Allmang, L.C. Feldman, W. van Saarlos, Experimental study of self-similarity in the coalescence growth regime, Phys. Rev. Lett. 68 (1992) 2358–2361.
[57] F.M. Ross, J. Tersoff, R.M. Tromp, Coarsening of self-assembled Ge quantum dots on Si(001), Phys. Rev. Lett. 80 (1998) 984–987.
[58] F.M. Ross, J. Tersoff, R.M. Tromp, M.C. Reuter, P.A. Bennett, Island growth of Ge on Si(001) and $CoSi_2$ on Si(111) studied with UHV electron microscopy, J. Electron Microsc. 48 (1999) 1059–1066.
[59] G. Medeiros-Ribeiro, A.M. Bratovski, T.I. Kamins, D.A.A. Ohlberg, R.S. Williams, Shape transition of Ge nanocrystals on a silicon (001) surface from pyramids to domes, Science 279 (1998) 353–355.
[60] T.I. Kamins, G. Medeiros-Ribeiro, D.A.A. Ohlberg, R.S. Williams, Evolution of Ge islands on Si(100) during annealing, J. Appl. Phys. 85 (1999) 1159–1171.
[61] CRC Handbook of Chemistry and Physics, 55th edition, CRC Press, Boca Raton, FL, 1974.
[62] J.P. Espinós, A. Fernández, R. González-Elipe, Oxidation and diffusion processes in nickel–titanium oxide systems, Surf. Sci. 295 (1993) 402–410.
[63] S. Bourgeois, F. Jomard, M. Perdereau, A SIMS study of nickel deposition on TiO_2(001): influence of the stoichiometry of the support, Surf. Sci. 249 (1991) 194–198.
[64] X. Lai, T.P. St. Clair, M. Valden, D.W. Goodman, Scanning tunnelling microscopy studies of metal clusters supported on TiO_2(110): morphology and electronic structure, Prog. Surf. Sci. 59 (1998) 25–52.
[65] M. Baumer, D. Cappus, H. Kuhlenbeck, H.-J. Freund, G. Wilhelmi, A. Brodde, H. Neddermeyer, The structure of thin NiO(100) films grown on Ni(100) as determined by low-energy-electron diffraction and scanning tunnelling microscopy, Surf. Sci. 253 (1991) 116–128.